Temperature-Dependent Rate Constants for the Reactions of Gas-Phase Lanthanides with O_2

Mark L. Campbell*,†

Chemistry Department, United States Naval Academy, Annapolis, Maryland 21402

Received: May 19, 1999; In Final Form: July 16, 1999

The reactivity of the gas-phase lanthanide atoms Ln (Ln = La−Yb with the exception of Pm) with O_2 is reported. Lanthanide atoms were produced by the photodissociation of [Ln(TMHD)$_3$] and detected by laser-induced fluorescence. For all the lanthanides studied with the exception of Yb, the reaction mechanism is bimolecular abstraction of an oxygen atom. The bimolecular rate constants (in molecule^{-1} cm^3 s^{-1}) are described in Arrhenius form by k[Ce($^1G_4$)] = $(3.0 \pm 0.4) \times 10^{-10} \exp(-3.4 \pm 1.3 \text{ kJ mol}^{-1}/RT)$; Pr($^4I_{9/2}$), $(3.1 \pm 0.7) \times 10^{-10} \exp(-5.3 \pm 1.5 \text{ kJ mol}^{-1}/RT)$; Nd($^5I_4$), $(3.6 \pm 0.3) \times 10^{-10} \exp(-6.2 \pm 0.4 \text{ kJ mol}^{-1}/RT)$; Sm($^7F_0$), $(2.4 \pm 0.4) \times 10^{-10} \exp(-6.2 \pm 1.5 \text{ kJ mol}^{-1}/RT)$; Eu($^8S_{7/2}$), $(1.7 \pm 0.3) \times 10^{-10} \exp(-9.6 \pm 0.7 \text{ kJ mol}^{-1}/RT)$; Gd($^9D_2$), $(2.7 \pm 0.3) \times 10^{-10} \exp(-5.2 \pm 0.8 \text{ kJ mol}^{-1}/RT)$; Tb($^6H_{15/2}$), $(3.5 \pm 0.6) \times 10^{-10} \exp(-7.2 \pm 0.8 \text{ kJ mol}^{-1}/RT)$; Dy($^5I_8$), $(2.8 \pm 0.6) \times 10^{-10} \exp(-9.1 \pm 0.9 \text{ kJ mol}^{-1}/RT)$; Ho($^4I_{15/2}$), $(2.4 \pm 0.4) \times 10^{-10} \exp(-9.4 \pm 0.8 \text{ kJ mol}^{-1}/RT)$; Er($^3H_6$), $(3.0 \pm 0.8) \times 10^{-10} \exp(-10.6 \pm 1.1 \text{ kJ mol}^{-1}/RT)$; Tm($^2F_{7/2}$), $(2.9 \pm 0.2) \times 10^{-10} \exp(-11.1 \pm 0.4 \text{ kJ mol}^{-1}/RT)$, where the uncertainties represent $\pm 2\sigma$. The reaction barriers are found to correlate to the energy required to promote an electron out of the 6s subshell. The reaction of Yb($^1S_0$) with O_2 reacts through a termolecular mechanism. The limiting low-pressure third-order rate constants are described in Arrhenius form by k_0[Yb($^1S_0$)] = $(2.0 \pm 1.3) \times 10^{-28} \exp(-9.5 \pm 2.8 \text{ kJ mol}^{-1}/RT)$ molecule^{-2} cm^6 s^{-1}.

Introduction

Studies of temperature-dependent rate constants for both the main group and transition metal reactions with O_2 in the gas phase have been extensive.[1−13] Atmospheric scientists are interested in these reactions owing to the presence of metallic species in the atmosphere from meteor ablation[14,15] and pollution from industrial smokestacks.[16] These reactions are also of interest in chemical vapor deposition processes.[17−19]

The mechanism for the reaction of a gas-phase metal atom with oxygen is dependent upon the thermodynamics of the process. About half of the naturally occurring metals are able to exothermically abstract an oxygen atom to form the metal monoxide. In the cases where the abstraction process is exothermic, the abstraction reaction is the observed mechanism while the reaction barriers are observed to be 15 kJ/mol or less.[2,9−13]

For many of the gas-phase metal atoms, the abstraction reaction is endothermic. Thus, at moderate temperatures, the termolecular reaction to produce the metal dioxide is the only viable process. The main group metals (with the exception of Ba, Ge, and Sn) and about half of the transition metals can only react with O_2 through the termolecular process. The termolecular kinetics of these atoms is quite diverse. Brown et al. reported on the 3d transition metal series and found that atoms with a ground or low-lying electronic state with a single electron in the valence s subshell react faster than those metals atoms with ground states with a filled outer s subshell.[3] This behavior has also generally been observed for the 4d and 5d transition metal series.[4−8]

Thus far, no experiments have been reported in the literature regarding the determination of bulk rate constants for neutral, gas-phase lanthanide metals with diatomic oxygen. In general, the chemistry of condensed-phase lanthanides is very similar. This similarity is due to the lanthanides differing only in the number of inner shell f electrons. It might be expected that since f electrons do not extend spatially as far as the outer 5d and 6s valence electrons, that the lanthanides' reactivity in the gas phase will be unaffected as the f electrons fill across the series. Here we report the first experiments determining the temperature-dependent rate constants of the neutral, gas-phase lanthanides reacting with O_2.

Experimental Section

The experimental arrangement has been described in detail elsewhere and will be described only briefly here.[20] Pseudo-first-order kinetic experiments ([Ln] ≪ [O_2]) were carried out in an apparatus with slowly flowing gas using a laser photolysis/laser-induced fluorescence (LIF) technique. Laser photolysis of a lanthanide metal precursor [Ln(TMHD)$_3$, where TMHD represents the 2,2,6,6-tetramethyl-3,5-heptanedionato ion] produced the gas-phase lanthanide metal atoms, and laser-induced fluorescence was used to probe their temporal behavior. The reaction chamber is a stainless steel reducing four-way cross with attached sidearms and a sapphire window for optical viewing. The reaction chamber is enclosed within a convection oven (Blue M, model 206F, T_{max} = 623 K) with holes drilled to allow for the exiting sidearms and the telescoping of the LIF signal to the PMT.

Lanthanide metal atoms were produced by the 248 nm photodissociation of the appropriate precursor with the focused output of an excimer laser (Lambda Physics Lextra 200). The focusing lens (f = 564 mm) was placed approximately one focal length from the reaction zone. The ground states of the

† Henry Dreyfus Teacher-Scholar.

10.1021/jp991647c
Published on Web 08/24/1999

TABLE 1: Laser-Induced Fluorescence Transitions Used to Probe the Ground State Lanthanide Atoms

lanthanide	wavelength (nm)[a]	lanthanide	wavelength (nm)[a]
Ce($^1G_4$)	491.532	Tb($^6H_{15/2}$)	432.643
Pr($^4I_{9/2}$)	513.344	Dy($^5I_8$)	421.172
Nd($^5I_4$)	492.453	Ho($^4I_{15/2}$)	405.393
Sm($^7F_0$)	380.394	Er($^3H_6$)	400.796
Eu($^8S_{7/2}$)	459.403	Tm($^2F_{7/2}$)	418.762
Gd($^9D_2$)	398.784	Yb($^1S_0$)	398.799

[a] Wavelengths taken from ref 21.

lanthanide metal atoms were detected via LIF using an excimer-pumped dye laser (Lambda Physics Lextra 50/ScanMate 2E). The wavelengths utilized to probe the ground state lanthanide atoms are listed in Table 1. The fluorescence was detected at 90° to the counterpropagated laser beams with a three-lens telescope imaged through an iris. Interference filters were used to isolate the LIF. A photomultiplier tube (Hamamatsu R375) was used in collecting the LIF which was subsequently sent to a gated boxcar sampling module (Stanford Research Systems SR250), and the digitized output was stored and analyzed by a computer. Real time viewing of the photolysis prompt emission and LIF signal were accomplished using a LeCroy model 9360 digital oscilloscope.

Nitrogen gas was used as the *primary* buffer gas; however, for the majority of lanthanides, a mixture of both N_2 and methane was used. As a result of their low vapor pressures at room temperature, the lanthanum precursors required heating in order to get enough precursor into the gas phase. The lanthanide metal precursor vapor was entrained in a flow of N_2 buffer gas. The diluted precursor, N_2 and CH_4 buffer gases and O_2 flowed through calibrated mass flow meters and flow controllers (MKS Types 1459C and 0258C, and Matheson models 8102 and 8202-1423) prior to admission to the reaction chamber. Each sidearm window was purged with a slow flow of buffer gas to prevent deposition of metal atoms and other photoproducts. Total flows varied between 250 and 900 sccm (sccm = standard cubic centimeters per minute); however, most experiments used a flow of approximately 700 sccm. Pressures were measured with MKS Baratron manometers, and chamber temperatures were measured with a thermocouple.

The delay time between the photolysis pulse and the dye laser pulse was varied by a digital delay generator (Stanford Research Systems DG535) controlled by a computer interfaced through a Stanford Research Systems SR245 computer interface. The trigger source for these experiments was scattered pump laser light incident upon a fast photodiode. LIF decay traces typically consisted of 200 data points, each point averaged from two to four laser shots.

Materials. The Ln(TMHD)$_3$ precursors were obtained from Strem Chemical. O_2 (MG Industries, 99.8%), CH_4 (Linde, ultrahigh purity grade, 99.99%), and N_2 (Potomac Airgas, Inc., 99.998%) were used as received.

Data Analysis and Results

The decay rates of the gas-phase lanthanide atoms as a function of oxygen pressure were investigated as a function of temperature. Under pseudo-first-order conditions in which no production processes occur after the initial photolysis event, the decrease in the [Ln] with time following the photolysis laser pulse is given by:

$$-\mathrm{d[Ln]}/\mathrm{d}t = (k_{obs}[O_2] + k_d)[\mathrm{Ln}] = (1/\tau)[\mathrm{Ln}] \qquad (1)$$

where k_{obs} is the observed rate constant due to O_2 at a fixed buffer gas pressure, k_d represents the depletion rate constant due to the reaction of the lanthanide metal with precursor molecules and fragments and diffusion out of the detection zone, and τ is the observed time constant for lanthanide metal depletion in the presence of a given [O_2], precursor, and buffer gas pressure. The LIF signal is proportional to the lanthanide metal number density, [Ln]. Thus, for a simple pseudo-first-order system in which production of excited states is insignificant, the LIF signal of the ground state at a time t after photolysis is

$$[\mathrm{Ln}](t) \propto \mathrm{LIF}(t) = \mathrm{LIF}_0 \exp(-t/\tau) \qquad (2)$$

where LIF_0 is the initial LIF signal immediately following the photolysis laser pulse. LIF decays which exhibit single-exponential behavior were fitted using a least-squares procedure to determine τ.

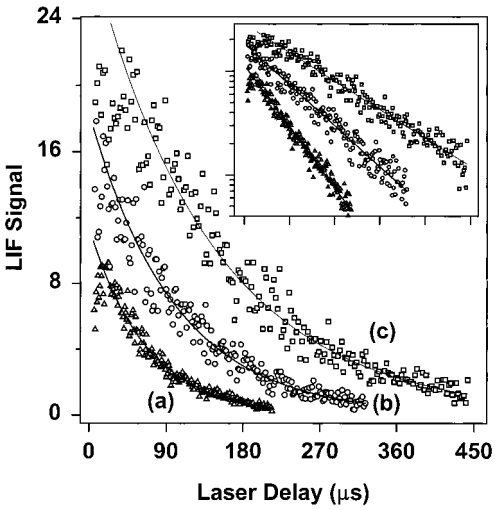

Figure 1. Typical decay curves with added O_2 at 448 K: (a) Tb($^6H_{15/2}$), P_{total} = 5.0 Torr, $P(O_2)$ = 12.4 mTorr, τ = 66.1 μs; (b) Nd($^5I_4$), P_{total} = 5.0 Torr, $P(O_2)$ = 4.9 mTorr, τ = 99.3 μs; (c) Er($^3H_6$), P_{total} = 20.0 Torr, $P(O_2)$ = 14.2 mTorr; τ = 143 μs. The solid lines through the data are exponential fits. The inset is a ln plot of the data.

In some cases, as a result of the photolysis of the lanthanide metal precursor, atoms in excited states are produced in significant quantities. Where possible, it is best to find a quencher gas to help relax excited states as rapidly as possible. Methane was used as a quencher gas for all of the lanthanides studied with the exception of Ce, Eu, Ho, and Yb. For a ground state in which quenching of excited states after the initial photolysis laser pulse is important, the time dependence of the ground state's concentration will exhibit biexponential behavior. For cases where the decay rate of an excited state down to the ground state is fast compared to the removal rate of the ground state, cascade processes are unimportant at long delay times and the ground state removal rate is determined by analysis of the decay at long times. Biexponential behavior of this type was observed for a few of the lanthanide metals. Typical plots of exponential decays are shown for terbium, neodymium, and erbium in Figure 1. For those lanthanides where growth was observed, time constants were determined by adjusting the range of the linear regression analysis; that is, the range did not include the beginning of the decay when growth was present. Decays were typically analyzed after a delay of up to one reaction lifetime and included data for a length of two to three reaction lifetimes

Once the reaction time constant has been determined for a series of oxygen number densities, the slope of a plot of $1/\tau$ vs

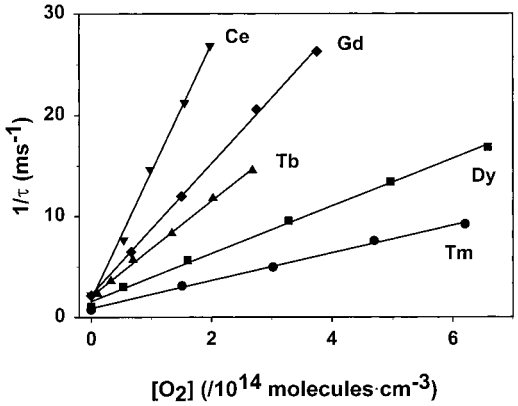

Figure 2. Typical plots for determining k_{second} for Ln + O_2 at 448 K. The solid line for each set of data is a linear regression fit from which k_{second} is obtained.

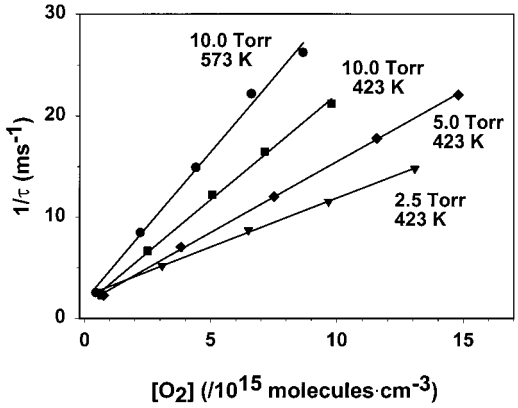

Figure 3. Typical plots for determining k_{second} for Yb($^1S_0$) + O_2 illustrating the third-order behavior of this reaction. The solid line for each set of data is a linear regression fit from which k_{second} is obtained.

$[O_2]$ yields the observed second-order rate constant, k_{obs}. Figure 2 illustrates examples of these types of plots for cerium, gadolinium, terbium, dysprosium, and erbium. The rate constants for the reaction of Yb with O_2 were found to be pressure dependent. The slopes of the linear fits in Figure 3 illustrate the pressure and temperature dependence of the second-order rate constants for this reaction. The relative uncertainty (i.e., the reproducibility) of the second-order rate constants is estimated at ±20% based on repeated measurements of rate constants under identical temperature and total pressure conditions. The absolute uncertainties are conservatively estimated to be ±30% and are based on the sum of the statistical scatter in the data, uncertainty in the flowmeter and flow controller readings (5%) and the total pressure reading (1%), uncertainties due to incomplete gas mixing, and uncertainties due to incomplete relaxation of the excited electronic states to the ground state.

Measured rate constants for the ground states of the lanthanides (with the exception of Pm and Yb) reacting with O_2 are listed in Table 2. The total pressure for the experiments involving Ce, Pr, Nd, Sm, Eu, Gd, and Tb was 5.0 Torr. The experiments involving Dy, Ho, Er, and Tm were performed at a total pressure of 20.0 Torr. Extensive pressure dependence studies were not performed; however, rate constants for Ce at 5 and 10 Torr at 373 K and Gd at 5 and 10 Torr at 348 K were found to be independent of total pressure within experimental uncertainty. An Arrhenius plot (ln k vs $1/T$) of the rate constants is shown in Figure 4. A fit of the rate constants for each

TABLE 2: Temperature Dependence of the Bimolecular Rate Constants (10^{-11} molecule^{-1} cm^3 s^{-1}) for the Reaction of Ln(g) + O_2(g) → LnO(g) + O(g)

T (K)	Ce	Pr	Nd	Sm	Eu	Gd	Tb	Dy	Ho	Er	Tm
298[a]			3.0		0.39		1.7	0.8	0.50	0.43	0.32
348	9.8	5.4	4.3		0.70	4.8	2.6	1.2	0.92	0.72	0.59
373	9.8	5.5	4.7	3.0	0.68	5.0	3.3	1.4	1.0	0.84	0.78
398	11.0	6.0	5.7	3.9	0.83	5.4	4.7	1.9	1.4	1.3	0.99
423	11.0	6.2	6.6	3.9	1.0	6.2	4.1	2.0	1.6	1.8	1.3
448	13.0	8.2	7.4	4.7	1.4	6.5	4.7	2.3	2.1	1.9	1.4
473	12.0	9.5	7.5	5.6	1.4	7.4	5.4	2.5	2.3	1.8	1.6
498	14.0	9.8	7.7	5.8	1.6	8.1	5.8	3.0	2.2	2.6	2.0
523		9.5	9.0	6.0	1.8	8.3	7.4	3.6	3.1	2.3	2.1
548		9.3	9.5	5.6	2.1		7.6	4.0	2.9	3.1	2.7
573		9.6	10.0	6.3	2.4		8.0	4.5	3.2	3.2	2.8
598			10.0		2.5		8.2	4.8	3.3	3.5	3.0
623			11.0				8.7		3.6	3.8	3.3

[a] Room-temperature varied from 296 to 300 K.

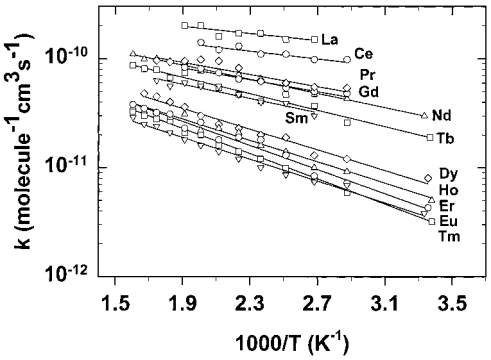

Figure 4. Arrhenius plots for the collisional disappearance of Ln with O_2. Each solid line is a linear regression fit of the rate constants to the equation $k(T) = A\,e^{-E_a/RT}$.

TABLE 3: Arrhenius Parameters and Promotion Energies for the Lanthanides

lanthanide	A (10^{-10} molecule^{-1} cm^3 s^{-1})	E_a (kJ/mol)	$6s^2-6s^1$ promotion energy (cm^{-1})[a]
La($^2D_{3/2}$)[b]	4.0 ± 0.6	3.1 ± 1.7	2668
Ce($^1G_4$)	3.0 ± 0.4	3.4 ± 1.3	2369
Pr($^4I_{9/2}$)	3.1 ± 0.7	5.3 ± 1.5	6714
Nd($^5I_4$)	3.6 ± 0.3	6.2 ± 0.4	8475
Sm($^7F_0$)	2.4 ± 0.4	6.2 ± 1.5	10801
Eu($^8S_{7/2}$)	1.7 ± 0.3	9.6 ± 0.7	12924
Gd($^9D_2$)	2.7 ± 0.3	5.2 ± 0.8	6378
Tb($^6H_{15/2}$)	3.5 ± 0.6	7.2 ± 0.8	8190
Dy($^5I_8$)	2.8 ± 0.6	9.1 ± 0.9	15567
Ho($^4I_{15/2}$)	2.4 ± 0.4	9.4 ± 0.8	15855
Er($^3H_6$)	3.0 ± 0.8	10.6 ± 1.1	16321
Tm($^2F_{7/2}$)	2.9 ± 0.2	11.1 ± 0.4	16742

[a] Reference 22. [b] Arrhenius parameters calculated from the rate constants in ref 2.

lanthanide to the equation $k(T) = A\,e^{-E_a/RT}$ was performed; the frequency factors, A, and activation energies, E_a, are listed in Table 3.

Measured rate constants for Yb($^1S_0$) with O_2 as a function of temperature and pressure are listed in Table 4. The low-pressure, third-order rate constants, k_0, for each temperature were approximated by fitting the second-order rate constants to a quadratic equation in buffer gas number density. The third-order rate constant was determined from the slope of the fit at [M] = 0. Representative fits of the data are shown in Figure 5, and the calculated k_0 values are listed in Table 4. A fit of the third-order rate constants to the Arrhenius equation yields $k_0 = (2.0 \pm 1.3) \times 10^{-28} \exp(-9.5 \pm 2.8\ \text{kJ mol}^{-1}/RT)$ molecule^{-2} cm^6 s^{-1} (Figure 6).

TABLE 4: Second-Order Rate Constants (10^{-12} molecule^{-1} cm^3 s^{-1}) and Low-Pressure Limiting Third-Order Rate Constants, k_0, (10^{-29} molecule^{-2} cm^6 s^{-1}) for the Reaction: Yb + O_2 + N_2 → YbO_2

T (K)	2.5 Torr	5.0 Torr	7.5 Torr	10.0 Torr	k_0
297	0.38	0.46	0.55	0.64	0.42 ± 0.12
373	0.58	0.84	1.1	1.3	0.86 ± 0.13
423	0.97	1.4	1.8	2.1	1.7 ± 0.2
473	0.86	1.2	1.5	1.8	1.6 ± 0.3
523	0.94	1.6	2.0	2.5	2.1 ± 0.3
573	1.3	2.2	2.6	2.9	3.4 ± 0.2
623	1.2	1.8	2.5	3.1	2.9 ± 0.5

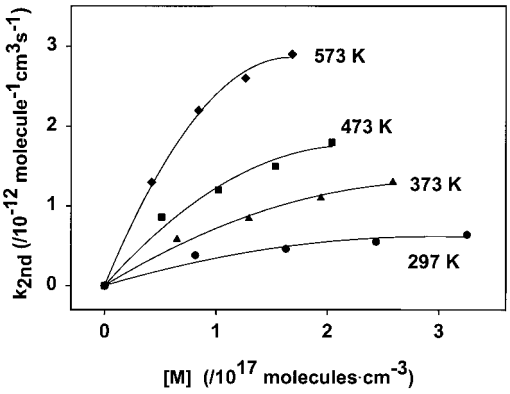

Figure 5. Pressure/temperature dependence of the reaction of Yb($^1S_0$) + O_2 in N_2 buffer. The solid lines are quadratic fits in [M]. The value of k_{third} (Table 3) for each temperature is determined from the slope of the fit at [M] = 0.

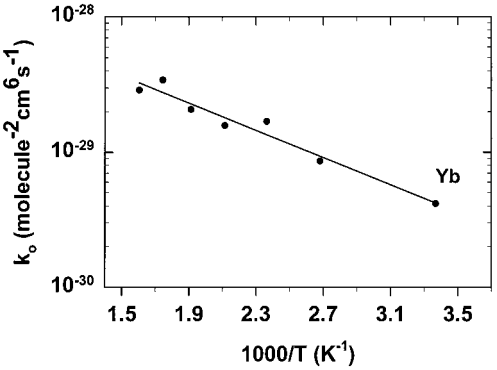

Figure 6. Arrhenius plot of the third-order rate constants for Yb($^1S_0$) with O_2. The solid line is a linear regression fit of the rate constants to the equation $k_0(T) = A\,e^{-E_a/RT}$.

Discussion

With the exception of europium and ytterbium, the abstraction reactions of the gas-phase lanthanides with oxygen are exothermic.[23,24] The Eu + O_2 reaction is approximately thermoneutral (ΔH = 12 ± 17 kJ/mol) so that the measured barrier might be partially due to a thermodynamic constraint. The Yb + O_2 reaction is 80 kJ/mol endothermic so that the abstraction reaction is precluded at moderate temperatures due to the thermodynamics of the process. Although extensive pressure-dependent studies were not performed for these reactions (with the exception of ytterbium), the instances in which pressure was varied indicated termolecular processes were unimportant. The Arrhenius behavior (i.e., activation energies of less than 15 kJ/mol and frequency factors near the gas kinetic collision rate) observed for these reactions is typical of the bimolecular abstraction mechanism seen with other metal atoms with O_2.[2,25,26] For the cases of Ce, Sm, Gd, Dy, and Ho, the metal oxide product has been directly observed from the reaction of the vaporized metal reacting with O_2.[27−31] Thus, an abstraction of an oxygen atom to produce the metal oxide is the indicated mechanism for all the lanthanides with the exception of ytterbium.

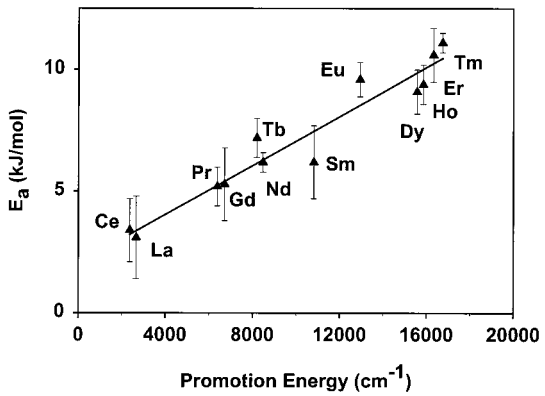

Figure 7. Plot of the experimental activation energies vs the electronic promotion energy from the ground state to the lowest energy state with a $6s^1$ electron configuration.

Energy barriers of only one of the lanthanides reported here have been previously reported for the abstraction reaction with oxygen. Using a beam−beam experiment, a threshold energy of 14.5 ± 1.9 kJ/mol was determined for the Eu + O_2 reaction.[32] This threshold value is slightly higher than the activation energy reported here; however, this threshold energy was determined from the translational energy component only so that a direct comparison with the value reported here cannot be made.

The experiments in this study indicate the gas-phase lanthanides show differences of up to almost 2 orders of magnitude in their rate constants for the reactions with oxygen. Similar to the results observed here, studies of gas-phase lanthanides with N_2O showed diverse kinetic behavior. In the study of the N_2O reactions, it was shown that the activation energies correlated with the excitation energy required to promote an s electron from an s^2 to an s^1 configuration.[33] Listed in Table 3 are the energies required to promote an electron from the ground state to a configuration with a single electron in the 6s subshell. Figure 7 shows there is a strong correlation between the measured activation energies and the $6s^2-6s^1$ promotion energies. Since the 6s orbital is the outermost valence orbital and the primary bonding orbital of the lanthanide, the interaction of the 6s orbital with O_2 is expected to be the dominant interaction at long range. The character of the potential upon the onset of orbital overlap will be determined by the interaction between the s orbital of the lanthanide and the singly occupied π^* antibonding orbitals of O_2. The ground states of the lanthanides are expected to be repulsive with O_2 because the 6s orbital in all the lanthanides is doubly occupied. Thus, the promotion of an electron out of the 6s subshell would be expected to reduce this repulsion. Our experimental results indicate the reduction of this repulsive interaction is important for these reactions since the activation energies are strongly correlated to the s^2-s^1 promotion energies.

The electronic structure of the lanthanides has been shown to be important in other bonding and kinetic circumstances. The trends in bond dissociation energies of the lanthanide monoxides can be accounted for nearly quantitatively by variations in electronic transition energies.[34−36] This model assumes the binding energies of the monoxides are nearly equal when the metal atom is in the $4f^{n-1}5d^1$ configuration so that the bond dissociation energy values for those metals requiring 4f−5d promotion are reduced below the baseline energy by the amount

of this promotion energy. This model actually assumes the metal oxide is described predominantly by the ionic structure $M^{2+}O^{2-}$, although the correlation between experimental and predicted values of the bond dissociation energies is quite good if the free atom values of the promotion energies are used.[36] In fact, Murad indicated that for praseodymium, the $Pr^{+}O^{-}$ structure is the more important configuration.[37] This structure results from the combination of the $4f^36s^1$ (Pr^+) and $2p^5$ (O^-) states. Thus, the requirement for reaction involves an ionic/covalent curve-crossing in which the covalent surface asymptotically correlates to the s^1 configuration. Therefore, the smaller the difference between the asymptotic energies of the lowest s^1 and s^2 energy states, the greater the probability of reaction. Murad's analysis was only for Pr because the spectroscopic data available was limited to Pr. However, the observed promotion energy relation might indicate the $M^{+}O^{-}$ structure is also important for the other lanthanide monoxides.

The reaction of the lanthanide ions with hydrocarbons also indicates a relationship between the reactivity and electron configuration. For the reactions of lanthanide ions with hydrocarbons,[38−42] it has been established that large variations in the activation of C−H and C−C bonds correlate with the energies required to promote a nonbonding 4f electron to a reactive 5d or 6s valence orbital. Insertion into a C−H or C−C bond apparently requires an electronic configuration on the metal center which is capable of forming two σ bonds. The f orbitals do not extend far enough spatially to be involved in the bonding; thus, the promotion of an f electron to a valence orbital is required to facilitate reaction. Thus, as the energy required to promote a metal ion electron from an f^ns^1configuration to an $f^{n-1}d^1s^1$ configuration increases, the activation barrier for the reaction increases. Thus, the rich chemistry of the gas-phase lanthanide atoms and ions appears to result from the variation in the electronic energy states in these systems.

The pressure dependence of the Yb + O_2 reaction indicates a termolecular addition reaction to produce YbO_2 with a barrier of 9.5 ± 2.8 kJ/mol. It is well-known that third-order reactions of closed-shell metal atoms with O_2 are characterized by an energy barrier. This barrier is located in the entrance channel at the crossing of the covalent and ionic potential energy surfaces.[43] With its $[Xe]4f^{14}6s^2$ configuration, ytterbium has the same filled outer s subshell as the alkaline earth metals. In its reaction with O_2, ytterbium is actually more similar to the other alkaline earths than barium. The abstraction reaction of barium with O_2 is exothermic and proceeds as a bimolecular process with a barrier of 7.06 ± 0.23 kJ/mol.[25] The abstraction reactions of magnesium, calcium, and strontium with O_2 are endothermic and not thermodynamically feasible at moderate temperatures. These alkaline earths are observed to undergo termolecular processes with O_2.[43−46] In each of these cases, a barrier has been observed from the temperature dependence of the limiting low-pressure, third-order rate constant. The barriers for magnesium, calcium, and strontium have been reported by Vinckier and co-workers as 16.8 ± 0.8, 10.2 ± 0.4, and 8.7 ± 0.6 kJ/mol, respectively.[43−45] Vinckier rationalized the trend in these barriers based on a model which assumes a partial charge transfer between the metal atom and oxygen molecule; that is, there should be a qualitative correlation between the activation energy and ionization energy. The ionization energies of Mg, Ca, Sr, and Yb are 7.64, 6.11, 5.69, and 6.25 eV, respectively.[22,47] The barrier observed here for ytterbium is similar to the barriers observed for calcium and strontium. The uncertainties in the activation energies precludes a more definite conclusion regarding the charge transfer mechanism.

Summary

We have measured the second-order rate constants as a function of temperature for the reactions of ground state lanthanide atoms with oxygen. With the exception of Yb, the gas-phase lanthanides abstract an oxygen atom to produce the metal oxide. Energy barriers vary from 3.4 for Ce($^1G_4$) to 11.1 kJ/mol for Tm($^2D_{3/2}$). The reaction barriers are found to correlate to the energy required to promote an electron out of the filled 6s subshell. The reaction of Yb($^1S_0$) with O_2 proceeds through a termolecular process with a barrier of 9.5 kJ/mol.

Acknowledgment. This research was supported by a Cottrell College Science Award of Research Corporation.

References and Notes

(1) Plane, J. M. C. In *Gas-Phase Metal Reactions*; Fontijn, A., Ed.; Elsevier: Amsterdam, 1992; p. 29.
(2) Campbell, M. L. *Chem. Phys. Lett*. **1998**, *294*, 339 and references therein.
(3) Brown, C. E.; Mitchell, S. A.; Hackett, P. A. *J. Phys. Chem.* **1991**, *95*, 1062.
(4) Campbell, M. L. *J. Chem. Soc., Faraday Trans.* **1996**, *92*, 4377 and references therein.
(5) Vinckier, C.; Christiaens, P.; Hendrickx, M. In *Gas-Phase Metal Reactions*; Fontijn, A., Ed.; Elsevier: Amsterdam, 1992; p 57.
(6) Campbell, M. L. *Laser Chem.* **1998**, *17*, 219.
(7) Helmer, M.; Plane, J. M. C. *J. Chem. Soc., Faraday Trans.* **1994**, *90*, 395.
(8) Campbell, M. L. *J. Chem. Soc., Faraday Trans.* **1998**, *94*, 353.
(9) Garland, N. L.; Nelson, H. H. *Chem. Phys. Lett.* **1992**, *191*, 269.
(10) LePicard, S. D.; Canosa, A.; Travers, D.; Chastaing, D.; Rowe, B. R.; Stoecklin, T. *J. Phys. Chem.* **1997**, *101*, 9988.
(11) Brown, A.; Husain, D. *Can. J. Chem.* **1976**, *54*, 4.
(12) Wiesenfeld, J. R.; Yuen, M. J. *J. Phys. Chem.* **1978**, *82*, 1225.
(13) Fontijn, A.; Bajaj, P. N. *J. Phys. Chem.* **1996**, *100*, 7085.
(14) Granier, C.; Jegou, J. P.; Megie, G. *Geophys. Res. Lett.* **1989**, *16*, 243.
(15) Plane, J. M. C. *Int. Rev. Phys. Chem.* **1991**, *10*, 55.
(16) Fontijn, A.; Blue, A. S.; Narayan, A. S.; Bajaj, P. N. *Combust. Sci. Technol.* **1994**, *101*, 59.
(17) Green, M. L.; Gross, M. E.; Papa, L. E.; Schnoes, K. J.; Brasen, D. *J. Electrochem. Soc.* **1985**, *132*, 2677.
(18) Ouyang, M.; Hiraoka, H. *Mater. Res. Bull.* **1997**, *32*, 1099.
(19) Jones, S. L.; Kumar, D.; Singh, R. K.; Holloway, P. H. *Appl. Phys. Lett.* **1997**, *71*, 404.
(20) Campbell, M. L.; McClean, R. E. *J. Chem. Soc., Faraday Trans.* **1995**, *91*, 3787.
(21) Meggers, W. F.; Corliss, C. H.; Scribner, B. F. *Tables of Spectral-Line Intensities, Part I Arranged by Elements*; NBS Monograph 145; U.S. Government Printing Office: Washington, DC, 1975.
(22) Martin, W. C.; Zalubas, R.; Hagan, L. Atomic Energy Levels—The Rare-Earth Elements. *Natl. Stand. Ref. Data Ser.* (U.S. Natl. Bur. Stand.) **1978**, NSRDS-NBS 60.
(23) Wagman, D. D.; Evans, W. H.; Parker, V. B.; Schumm, R. H.; Halow, I.; Bailey, S. M.; Churney, K. L.; Nuttall, R. L. *J. Phys. Chem. Ref. Data* **1982**, *11* (Suppl. 2).
(24) Pedley, J. B.; Marshall, E. M. *J. Phys. Chem. Ref. Data* **1983**, *12*, 967.
(25) Nien, C.-F.; Plane, J. M. C. *J. Phys. Chem.* **1991**, *94*, 7193.
(26) Campbell, M. L. *J. Phys. Chem. A* **1998**, *102*, 892.
(27) Linton, C.; Dulick, M.; Field, R. W.; Leyland, P. C.; Barrow, R. F. *J. Mol. Spectrosc.* **1983**, *102*, 441.
(28) Linton, C.; Bujin, G.; Rana, R. S.; Gray, J. A. *J. Mol. Spectrosc.* **1987**, *126*, 370.
(29) Carette, P.; Hocquet, A.; Douay, M.; Pinchemel, B. *J. Mol. Spectrosc.* **1987**, *124*, 243.
(30) Linton, C.; Gaudet, D. M.; Schall, H. *J. Mol. Spectrosc.* **1983**, *102*, 441.
(31) Liu, Y. C.; Linton, C.; Schall, H.; Field, R. W. *J. Mol. Spectrosc.* **1984**, *104*, 72.
(32) Dirscherl, R.; Michel, K. W. *Chem. Phys. Lett.* **1976**, *43*, 547.
(33) Campbell, M. L. *J. Chem. Phys.* **1999**, *111*, 562.
(34) Ames, L. L.; Walsh, P. N.; White, D. *J. Phys. Chem.* **1967**, *71*, 2707.
(35) Hildenbrand, D. L. *Chem. Phys. Lett.* **1977**, *48*, 340.
(36) Murad, E.; Hildenbrand, D. L. *J. Chem. Phys.* **1980**, *73*, 4005.
(37) Murad, E. *Chem. Phys. Lett.* **1978**, *59*, 359.

(38) Schilling, J. B.; Beauchamp, J. L. *J. Am. Chem. Soc*. **1988**, *110*, 15.
(39) Yin, W. W.; Marshall, A. G.; Marcalo, J.; de Matos, A. P. *J. Am. Chem. Soc*. **1994**, *116*, 8666.
(40) Cornehl, H. H.; Heinemann, C.; Schroder, D.; Schwarz, H. *Organometallics* **1995**, *14*, 992.
(41) Gibson, J. K. *J. Phys. Chem*. **1996**, *100*, 15688.
(42) Gibson, J. K.; Haire, R. G. *J. Phys. Chem. A* **1998**, *102*, 10746.
(43) Vinckier, C.; Helaers, J. *J. Phys. Chem. A* **1998**, *102*, 8333.
(44) Vinckier, C.; Christiaens, P. *Bull. Soc. Chim. Belg.* **1992**, *101*, 10.
(45) Vinckier, C.; Remeysen, J. *J. Phys. Chem.* **1994**, *98*, 10535.
(46) Nien, C.-F.; Rajasekhar, B.; Plane, J. M. C. *J. Phys. Chem.* **1993**, *97*, 6449.
(47) Moore, C. E. Atomic Energy Levels as Derived from the Analysis of Optical Spectra. *Natl. Stand. Ref. Data Ser*. (U.S. Natl. Bur. Stand.) **1971**, NSRDS-NBS 35; Vols. I and II.